Journal of Computational Physics: X 11 (2021) 100090

Contents lists available at ScienceDirect

Journal of Computational Physics: X

www.elsevier.com/locate/jcpx

A cut finite element method for non-Newtonian free surface flows in 2D - application to glacier modelling

Josefin Ahlkrona [a,b,*], Daniel Elfverson [c]

[a] Department of Mathematics, Stockholm University, Stockholm, Sweden
[b] Swedish e-Science Research Centre (SeRC), Stockholm, Sweden
[c] Department of Mathematics and Mathematical Statistics, Umeå University, Umeå, Sweden

ARTICLE INFO

Article history:
Received 27 August 2020
Received in revised form 25 February 2021
Accepted 4 April 2021
Available online 15 April 2021

Keywords:
Ice sheet modelling
CutFEM
Free boundary problems
Non-Newtonian flow
Unfitted finite element methods
Sharp interface methods

ABSTRACT

In ice sheet and glacier modelling, the Finite Element Method is rapidly gaining popularity. However, constructing and updating meshes for ice sheets and glaciers is a non-trivial and computationally demanding task due to their thin, irregular, and time dependent geometry. In this paper we introduce a novel approach to ice dynamics computations based on the unfitted Finite Element Method CutFEM, which lets the domain boundary cut through elements. By employing CutFEM, complex meshing and remeshing is avoided as the glacier can be immersed in a simple background mesh without loss of accuracy. The ice is modelled as a non-Newtonian, shear-thinning fluid obeying the p-Stokes (full Stokes) equations with the ice atmosphere interface as a moving free surface. A Navier slip boundary condition applies at the glacier base allowing both bedrock and subglacial lakes to be represented. Within the CutFEM framework we develop a strategy for handling non-linear viscosities and thin domains and show how glacier deformation can be modelled using a level set function. In numerical experiments we show that the expected order of accuracy is achieved and that the method is robust with respect to penalty parameters. As an application we compute the velocity field of the Swiss mountain glacier Haut Glacier d'Arolla in 2D with and without an underlying subglacial lake, and simulate the glacier deformation from year 1930 to 1932, with and without surface accumulation and basal melt.

1. Introduction

As the atmosphere and ocean is warming, ice sheets and glaciers melt. The meltwater causes global mean sea level to rise, and has the potential to alter ocean circulation [1,2]. Ice behaves as a very viscous, non-Newtonian, shear-thinning fluid, and in order to predict future melt rates it is crucial to be able to accurately simulate how it flows and deforms. Ice sheet and glacier modelling is thus a very important moving boundary, non-linear, fluid mechanics problem.

Due to the complex and changing geometries involved, the Finite Element Method (FEM) is gaining popularity in ice modelling since it allows for unstructured meshes [3–6]. Ice sheet and glacier models employ traditional *fitted* FEM, that is, the computational mesh is fitted to the model domain with nodes placed on the boundary. However, there is a limit to just how complex moving domains fitted FEM can handle. Requiring mesh nodes to align with the boundary involves non-

* Corresponding author.
E-mail address: ahlkrona@math.su.se (J. Ahlkrona).

https://doi.org/10.1016/j.jcpx.2021.100090

trivial mesh construction, and as the domain moves either costly remeshing or problems with low quality mesh elements if the mesh is simply distorted. In ice modelling the initial mesh is usually constructed by creating a 2D triangulation in the horizontal plane and extruding it in the vertical direction into a number of layers. Because glaciers are thinner than they are wide, the resulting prismatic elements become very flat. At land based ice margins the thickness of elements even goes towards zero or some artificial minimum thickness, and when the ice/atmosphere interface moves, the mesh is usually distorted to fit the boundary, which can comprise element quality even more. At the coast, the extruded mesh approach renders ice cliffs at the coast exactly vertical, which is not always true in reality. Furthermore, when the margins of the ice sheet move the mesh may have to be completely reconstructed, which is a costly procedure. Ice sheet margins may move suddenly, e.g when ice breaks off into ice bergs, and in long simulations there can even be topological changes if the ice melts into separate islands.

In recent years, more robust alternatives to traditional fitted FEM has been developed; unfitted sharp interface methods [7,8]. Unfitted methods does not rely on placing mesh nodes on the boundary, but rather immerses the domain onto a background mesh, letting the boundary cut through elements. Apart from avoiding generation and repeated update of complex meshes, unfitted methods also allows for topological changes. In this paper we extend the unfitted FEM method called CutFEM [7], so that it can be used for ice modelling.

CutFEM relies on implementing boundary conditions weakly using Nitsche's method [9]. Using only Nitsche's method with an unfitted mesh would typically result in losing half an order of convergence [10]. CutFEM instead keeps accuracy by employing quadrature only over the physical domain, combined with extra stabilisation terms. CutFEM has successfully been applied to Stokes and Navier-Stokes flow [11,12], but modelling ice requires us to extend the method to the strongly non-linear p-Stokes (or full Stokes) equations which describes non-Newtonian flow, and to adapt the method to the thinness and sharp corners of ice domains. In this paper we describe how this can be done and prove the accuracy of our method through numerical experiments in MATLAB. We implement a level-set method for moving the ice/atmosphere interface and show how to represent variable sliding at the base of the ice. Nitsche's method and the level-set method has successfully been applied to ice dynamics modelling in e.g. [13,14] for parts of the boundary (the calving front and grounding line), but outside the framework of CutFEM. The advantage of using CutFEM is that optimal accuracy is kept.

The paper is organised as follows. In Section 2 we describe the non-linear equations governing ice flow together with the equation that describes the moving boundary. In Section 3 the CutFEM method is outlined, including how the non-linear material properties, thin domains and basal sliding conditions are handled. Section 4 explains the implementation of the level set method and how glacier margins are handled as the ice moves. In Section 5 we perform four numerical experiments: one unit square test to ensure that the order of accuracy is kept and that the accuracy is robust with respect to penalty parameters, and six experiments modelling the Swiss mountain glacier Haut Glacier d'Arolla, which is part of the ice sheet modelling bench mark experiment ISMIP-HOM [15].

2. Governing equations and boundary conditions

Glacier and ice sheet flow is governed by a non-linear version of the Stokes equations called the *p-Stokes* equations or *full Stokes* equations,

$$\left.\begin{aligned} -\nabla\cdot\mathbf{S}(\mathbf{Du}) + \nabla p &= \rho\mathbf{g} \\ \nabla\cdot\mathbf{u} &= 0 \end{aligned}\right\} \quad \text{in } \Omega. \tag{1}$$

Here $\mathbf{u} = (u_x, u_y)$ is the velocity field in a two dimensional Cartesian coordinate system (x, y), p is the pressure, $\Omega \in \mathbb{R}^2$ is an open, two-dimensional bounded domain, and $\rho\mathbf{g}$ is the force of gravity. The stress tensor is denoted by $\mathbf{S}$ and depends on the strain rate tensor $\mathbf{Du} = (\nabla\mathbf{u} + (\nabla\mathbf{u})^T)/2$ as

$$\mathbf{S}(\mathbf{Du}) = 2\mu\mathbf{Du}. \tag{2}$$

Since ice is a non-Newtonian, shear-thinning material, the viscosity μ depends on the Frobenius norm of the strain rate

$$\mu = \frac{1}{2}A^{1-\mathfrak{p}}(\epsilon_{crit}^2 + \frac{1}{2}||\mathbf{Du}||_F^2)^{\frac{\mathfrak{p}-2}{2}}. \tag{3}$$

The material parameter $\mathfrak{p}$ lies in the interval $(1, 2)$ for shear-thinning fluids, meaning the viscosity is very large where the strain rate is low. A small $\mathfrak{p}$ corresponds to a strong non-linearity while $\mathfrak{p} = 2$ models a linear, Newtonian fluid. For ice $\mathfrak{p} = 4/3$ is the standard choice, which in glaciology terminology corresponds to the Glen parameter being $n_{Glen} = 3$. The small regularisation parameter ϵ_{crit} is included to avoid numerical problems in cases when the Frobenius norm of the strain rate tensor $||\mathbf{Du}||_F^2$ approaches zero. The rate factor $A = A(T)$ models how ice viscosity depends on the temperature T. We consider isothermal condition and so that A is a constant.

The natural velocity and pressure spaces for weak solutions of the full Stokes equations are $[W^{1,\mathfrak{p}}(\Omega)]^2$ and $L^{\mathfrak{p}'}(\Omega)$ respectively, where L^{ν} denotes a Lebesgue space and $W^{1,\nu}$ a Sobolev space of order one. The parameter $\mathfrak{p}'$ relates to $\mathfrak{p}$ as $\mathfrak{p}' = \mathfrak{p}/(\mathfrak{p}-1)$, see e.g. [16,17]. Note that in a linear setting $\mathfrak{p} = \mathfrak{p}' = 2$ and the spaces are consistent with those associated with the linear Stokes equations.

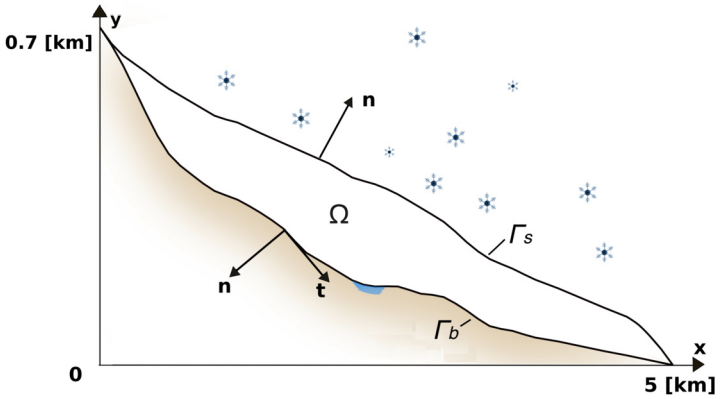

Fig. 1. A cross-section of the mountain glacier Haut Glacier d'Arolla. The outwards pointing normal is denoted by **n** and the tangential vector by **t**. The base Γ_b rests partly on bedrock (brown) and partly on subglacial water (blue). The surface Γ_s evolves in time due to ice deformation and precipitation/melting.

The glacier boundary $\Gamma = \partial\Omega$ is divided into two parts, Γ_s and Γ_b, denoting the interface between the ice and the atmosphere (ice surface) and the interface between the ground and the ice respectively, see Fig. 1. The ice surface Γ_s is a free boundary, which in glaciology is typically described by a height function $z = h(x,t)$ indicating the elevation of Γ_s at a certain horizontal position x at a time t. In this paper we will instead use a level-set formulation, which unlike the height function formulation does not require that there is a unique z for each x, nor excludes topological changes. The position of the surface is thus indicated by a level set function $\Phi(x,z,t)$ which is zero at the surface Γ_s. The evolution of the surface is given by the evolution equation

$$\frac{\partial \Phi}{\partial t} + \mathbf{u}\cdot\nabla\Phi = a_s, \tag{4}$$

where a_s is an accumulation/ablation function depending on the atmospheric conditions such as e.g. snow. As customary in glaciology the accumulation/ablation is added only in the vertical direction (since precipitation and ablation comes from above), i.e. $a_s = -a_s^{\perp}\nabla\Phi$, $a_s^{\perp}$ being materia added or removed in the z-coordinate direction.

The boundary condition for the full Stokes equations at the free surface is

$$(-p\mathbf{I} + 2\mu\mathbf{Du})\mathbf{n} = \mathbf{0} \text{ on } \Gamma_s, \tag{5}$$

where $\mathbf{n}$ is the outwards pointing unit normal of the domain boundary and $\mathbf{I}$ is the identity matrix. At the base Γ_b the ice can either be frozen to the ground or it can be sliding on sediments or water so that a Navier slip type condition applies

$$\mathbf{P^n}(\mathbf{u} - \mathbf{g_d}) = \mathbf{0} \quad \text{on } \Gamma_b, \tag{6}$$

$$\mathbf{P^t}(\epsilon(2\mu\mathbf{Dun} - \mathbf{d}) + \mu(\mathbf{u} - \mathbf{g_d})) = \mathbf{0} \quad \text{on } \Gamma_b. \tag{7}$$

Here the projection matrices $\mathbf{P^n}, \mathbf{P^t} \in \mathbb{R}^{2\times 2}$ defines the projection to the normal and tangential plane and are given as $\mathbf{P^n} = \mathbf{n}\otimes\mathbf{n}$ and $\mathbf{P^t} = \mathbf{I} - \mathbf{n}\otimes\mathbf{n}$, where $\otimes$ denotes an outer product. We set $\mathbf{d} = \mathbf{0}$, meaning there is zero traction at the base, and will from now on omit $\mathbf{d}$ from the equations. The term $\mathbf{g}_d = (0, -a_b^{\perp})$ models melt or refreezing at the base of the glacier. The slip length ϵ determines the amount of slip in the tangential direction. For $\epsilon = 0$ equations (6)-(7) reduce to a homogeneous Dirichlet condition, valid for the case when the ice is frozen to underlying base. When $\epsilon \to \infty$ a free slip condition is retrieved, which is valid when the ice is slipping over water. An intermediate slip length ϵ results in a mixed Robin condition, which describes situations when the ice is not frozen at the base or is resting on deformable debris/sediments. The Navier slip boundary conditions of equation (6)-(7) were formulated in a CutFEM framework by [18] for the linear Stokes equations ($\mathfrak{p} = 2$).

3. CutFEM formulation

3.1. Computational mesh and finite element spaces

The physical domain Ω is immersed in a larger a rectangular domain Ω_0, i.e. $\Omega \subset \Omega_0 \subset \mathbb{R}^2$, see Fig. 2a. This larger domain is easy to partition into a structured so called *background mesh* $\mathcal{T}_{0,h}$ consisting of rectangles K, where h denotes the cell diameter. For the Arolla glacier, the background meshes, $\mathcal{T}_{0,h}$ are slightly anisotropic to accommodate the thin Arolla glacier, unlike the background meshes used so far in the framework of CutFEM. Elements are thus eight times longer in the x-direction than in the y-direction, reflecting the thinness of the glacier (see Fig. 1). The discrete solution will be sought

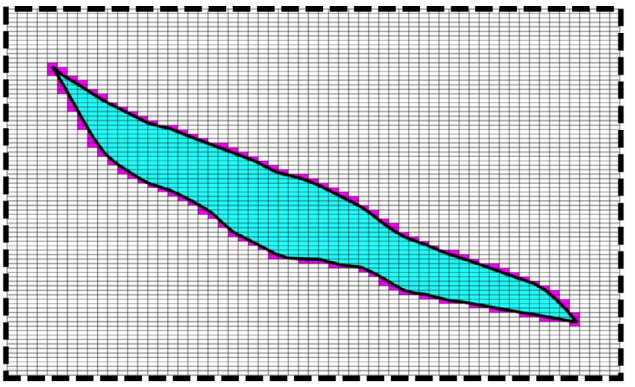

(a) The physical domain (cyan) is immersed in the larger rectangular domain Ω_0 (indicated by the dashed line).

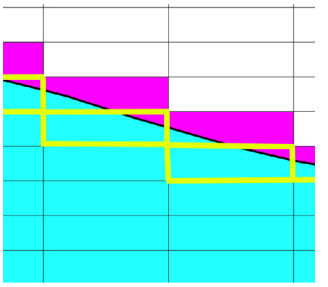

(b) A zoomed in view of the upper boundary. Interior facets that are cut by the boundary, $\mathcal{F}_h(\Gamma)$, are marked yellow.

Fig. 2. A mesh for the Arolla glacier. The cyan part marks the physical domain Ω. The thin black lines marks the mesh faces for the background mesh constructed on Ω_0 and the magenta and cyan together marks the active part of the mesh, $\mathcal{T}_h(\Omega)$. Note that the picture is stretched in the vertical direction, so that in reality the elements are slightly anisotropic.

only on the active part of the mesh, defined as all elements which are intersected by the domain Ω, i.e.

$$\mathcal{T}_h(\Omega) = \{K \in \mathcal{T}_{0,h} : K \cap \Omega(t) \neq \emptyset\}. \tag{8}$$

The active mesh is marked cyan and magenta in Fig. 2a. We call the union of the elements in the active part of the mesh the active domain $\Omega_h(t) = \cup_{K\in\mathcal{T}_h} K$. The facets of the elements in $\mathcal{T}_h(\Omega)$ enters in the formulation of stabilisation terms and we therefore introduce the some notations for these. All facets belonging to elements in $\mathcal{T}_h(\Omega)$ are denoted by $\mathcal{F}_h(\Omega)$ and all *interior* facets, i.e facets that are shared by two elements that are *both* in $\mathcal{T}_h(\Omega)$ are denoted by $\mathcal{F}_{i,h}(\Omega)$. The interior facets will be used for stabilising the pressure (i.e. for inf-sup stabilisation). The elements and facets $\mathcal{T}_h(\Gamma)$ and $\mathcal{F}_h(\Gamma)$ which are intersected, or "cut", by the boundary Γ are of extra importance, as it is on these facets that extra stabilisation terms are needed for the CutFEM formulation. These elements and facets are defined as

$$\mathcal{T}_h(\Gamma) = \{K \in \mathcal{T}_h(\Omega) : \overline{K} \cap \Gamma \neq \emptyset\}, \tag{9}$$

$$\mathcal{F}_h(\Gamma) = \{F \in \mathcal{F}_{i,h}(\Omega) : K_F^+ \cap \Gamma \neq 0 \text{ or } K_F^- \cap \Gamma \neq 0\}, \tag{10}$$

where K_F^+ and K_F^- are the two elements that share the facet F. In Fig. 2b facets belonging to $\mathcal{F}_h(\Gamma)$ are marked yellow.

On the background mesh Ω_0 we introduce a finite element space of bi-linear, continuous functions

$$X_{0,h} := \left\{\omega \in C(\overline{\Omega_0});\ \omega_K \circ F_K \in \mathbb{Q}_1(\hat{K}),\ K \in \mathcal{T}_{0,h}\right\}, \tag{11}$$

where the space $\mathbb{Q}_1(\hat{K}) := span\{\hat{x}, \hat{y}, \hat{x}\hat{y}, (\hat{x}, \hat{y}) \in \hat{K}\}$ is defined on the reference element $\hat{K} := (0, 1)^d$. The mapping F_K maps from the reference element to an element K, and will for the numerical experiments on the Arolla glacier geometry represent a slight compression of the grid in the vertical direction. The finite element space on the active domain is defined as the restriction of $X_{0,h}$ onto Ω_h

$$X_h = X_{0,h}|_{\Omega_h}. \tag{12}$$

This space is used to approximate both the velocity and pressure solution

$$\boldsymbol{\mathcal{X}}_h = [X_h]^2, \quad \mathcal{Q}_h = X_h, \tag{13}$$

that is, we employ equal order bilinear elements on the active mesh.

3.2. Discrete problem

The discretized problem now reads: Find velocity and pressure $(\mathbf{u}, p_h) \in \boldsymbol{\mathcal{X}}_h \times \mathcal{Q}_h$ so that

$$\begin{aligned} &a_h(\mathbf{u}_h, \mathbf{v}_h) + b(p_h, \mathbf{v}_h) - b(q_h, \mathbf{u}_h) + s_p(p_h, q_h) \\ &\quad + g_u(\mathbf{u}_h, \mathbf{v}_h) + g_p(\mathbf{u}_h, \mathbf{v}_h) = l_h(\mathbf{u}_h, \mathbf{v}_h) \quad \forall (\mathbf{v}_h, q_h) \in \boldsymbol{\mathcal{X}}_h \times \mathcal{Q}_h, \end{aligned} \tag{14}$$

where a_h stems from the stress tensor in (1), the two b_h stems from the pressure gradient and from the divergence free constraint, s_h is an inf-sup stabilisation needed as we employ equal order elements, g_u, and g_p are the extra stabilisation terms called *ghost penalty terms* needed for the CutFEM formulation, and l_h represents the right hand side of (1). We will now describe each of these terms in detail.

3.2.1. Nitsche terms

Following [18] the form $a_h(\mathbf{u}_h, \mathbf{v}_h)$ contains the viscous term together with several extra boundary terms that are required for imposing the Dirichlet or Navier-slip boundary conditions (6)-(7) weakly on a boundary that cuts the mesh.

$$\begin{aligned} a_h(\mathbf{u}_h, \mathbf{v}_h) &:= (2\mu \mathbf{D}\mathbf{u}_h, \mathbf{D}\mathbf{v}_h)_\Omega - \langle 2\mu \mathbf{D}\mathbf{u}_h \mathbf{n}, \mathbf{v}_h \rangle_{\Gamma_b} - \langle \mathbf{P^n} \mathbf{u}_h, 2\mu \mathbf{D}\mathbf{v}_h \mathbf{n} \rangle_{\Gamma_b} \\ &+ \langle \frac{2\mu}{\gamma^n h_\Gamma} \mathbf{u}_h \cdot \mathbf{n}, \mathbf{v}_h \cdot \mathbf{n} \rangle_{\Gamma_b} + \langle \frac{\epsilon}{\epsilon + \gamma^t h_\Gamma} \mathbf{P^t}(2\mu \mathbf{D}\mathbf{u}_h \mathbf{n}), \mathbf{v}_h \rangle_{\Gamma_b} + \langle \frac{\mu}{\epsilon + \gamma^t h_\Gamma} \mathbf{u}_h \cdot \mathbf{t}, \mathbf{v}_h \cdot \mathbf{t} \rangle_{\Gamma_b} \\ &- \langle \frac{\epsilon \gamma^t h_\Gamma}{\epsilon + \gamma^t h_\Gamma} \mathbf{P^t}(2\mu \mathbf{D}\mathbf{u}_h \mathbf{n}), 2\mathbf{D}\mathbf{v}_h \mathbf{n} \rangle_{\Gamma_b} - \langle \frac{\mu \gamma^t h_\Gamma}{\epsilon + \gamma^t h_\Gamma} \mathbf{P^t} \mathbf{u}_h, 2\mathbf{D}\mathbf{v}_h \mathbf{n} \rangle_{\Gamma_b}. \end{aligned} \tag{15}$$

The second term comes from the partial integration associated with writing (1) on weak form. Note that unlike for standard fitted FEM, this term is non-zero even for Dirichlet conditions since $\mathbf{v}$ is non-zero on Γ_b. The term makes the form unsymmetric, which with Nitsche's method is remedied by adding extra terms to symmetrize the problem. For no-slip conditions ($\epsilon \to 0$) the third and last term together constitutes these symmetrisation terms. The fourth and sixth term are penalty terms that impose the Dirichlet condition, and γ^t and γ^n are Nitsche penalty parameters in the tangential and normal direction. The lower these parameters are, the more emphasis is put on imposing the boundary conditions, versus fulfilling the equations. For $\epsilon \to \infty$ we retrieve the free slip condition. In this case it is the second to last term that is the penalty term imposing the boundary condition. For a more detailed discussion of these terms, we refer to [18]. Note that for ice, the viscosity in each of these terms is variable in time and space, unlike in the formulation in [18]. The measure h_Γ differs from [18] where the cellsize h is used instead. Since for anisotropic elements it matters if the boundary Γ cuts an element along the long side or short side, we define $h_\Gamma = h_x h_y / (h_x \mathbf{t}_{\Gamma,x} + h_y \mathbf{t}_{\Gamma,y})$, where $\mathbf{t}_\Gamma$ is the average tangential to Γ within an element. For the Arolla glacier, the boundary mostly cuts the cells along the long edge of elements, so that $h_\Gamma \approx h_y$. This choice can be motivated by revising the trace and inverse inequalities involved in the CutFEM stability proofs and will be presented thoroughly in a separate publication.

For the pressure/divergence constraint form b_h one extra boundary term enters, stemming from the partial integration

$$b_h(p_h, \mathbf{v}_h) := b(p_h, \mathbf{v}_h) + \langle p, \mathbf{v} \cdot \mathbf{n} \rangle_{\Gamma_b}. \tag{16}$$

Finally, given that $\mathbf{d}$ is zero in (6)-(7), the right hand side form is

$$\begin{aligned} l_h(\mathbf{u}, \mathbf{v}) &:= (\mathbf{f}, \mathbf{v})_\Omega - \langle \mathbf{g}_d \cdot \mathbf{n}, (2\mu \mathbf{D}\mathbf{v}_h \mathbf{n}) \cdot \mathbf{n} \rangle_{\Gamma_b} + . \langle \frac{2\mu}{\gamma^n h_\Gamma} \mathbf{g}_d \cdot \mathbf{n}, \mathbf{v}_h \cdot \mathbf{n} \rangle_{\Gamma_b} \\ &- \langle \mathbf{g}_d \cdot \mathbf{n}, q_h \rangle_{\Gamma_b} + \langle \frac{\mu}{\epsilon + \gamma^t h_\Gamma} \mathbf{g}_d \cdot \mathbf{t}, \mathbf{v}_h \cdot \mathbf{t} \rangle_{\Gamma_b} - \langle \frac{\mu \gamma^t h_\Gamma}{\epsilon + \gamma^t h_\Gamma} \mathbf{P^t} \mathbf{g}_d, 2\mathbf{D}\mathbf{v}_h \mathbf{n} \rangle_{\Gamma_b} \end{aligned} \tag{17}$$

Note that even though the finite element spaces are defined on the entire active domain Ω_h, the integrations in (15)-(17) are only over Ω for accuracy reasons. The contribution to the final FEM matrices of the cut elements may thus be very small (see Fig. 2b), which would lead to bad condition numbers of these matrices and stability issues were it not for g_u, and g_p.

3.2.2. Stabilisation terms

The ghost penalty stabilisation terms g_u and g_p that are added to handle issues related to small cut elements are defined as

$$g_u(\mathbf{u}_h, \mathbf{v}_h) = \beta_u \sum_{F \in \mathcal{F}_h(\Gamma)} h_n \langle [\![\mathbf{n}_f \cdot \nabla \mathbf{u}_h]\!], [\![\mathbf{n}_F \cdot \nabla \mathbf{v}_h]\!] \rangle_F, \tag{18}$$

$$g_p(p_h, q_h) = \beta_p \sum_{F \in \mathcal{F}_h(\Gamma)} \frac{h_n^3}{\mu} \langle [\![\mathbf{n}_F \cdot \nabla p_h]\!], [\![\mathbf{n}_F \cdot \nabla p_h]\!] \rangle_F, \tag{19}$$

where h_n and h_t is the length of the side normal and tangential to the facet F (see Fig. 3), $\mathbf{n}_F$ is the normal vector to the facet, β_u and β_p are user defined parameters and $[\![\phi]\!] := (\phi_F^+ - \phi_F^-)$ denotes the jump of a quantify (ϕ), where $\phi^\pm(x, y) := \lim_{t \to 0^+} \phi((x, y) \pm t\mathbf{n}_F)$. The ghost penalties penalise jumps in pressure and velocity gradients across facets belonging to $\mathcal{F}_h(\Gamma)$. These stabilisation terms are an anisotropic version of the isotropic ghost penalty terms in [11], as we need slightly anisotropic background meshes to accommodate the thin Arolla glacier. The formulation can be found by following the standard CutFEM stability proof and tracking the length of the normal and tangential part in the trace and inverse inequalities separately.

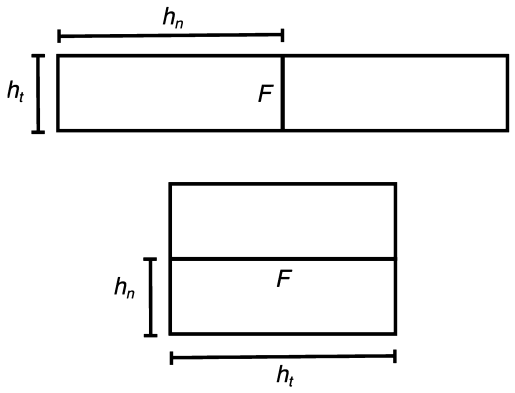

Fig. 3. The length of the sides of each cell is denoted by h_t if it is parallel to the facet F, and h_n if it is perpendicular.

The term $s_p(\mathbf{u}_h, \mathbf{v}_h)$ in (14) is a stabilisation term of Continuous Interior Penalty (CIP) type [19]

$$s_p(p_h, q_h) = \alpha \sum_{F \in \mathcal{F}_h(\Omega)} \frac{h_x^2 h_n}{\mu} \langle [\![\mathbf{n}_F \cdot \nabla p_h]\!], [\![\mathbf{n}_F \cdot \nabla p_h]\!] \rangle_F, \tag{20}$$

where α is a user defined parameter. This stabilisation is needed since the equal order spaces $\mathcal{X}_h$ and $\mathcal{Q}_h$ are well-known to violate the inf-sup condition [20]. Also here we have modified the formulation to suit anisotropic meshes. The form of the stabilisation is consistent with the anisotropic stabilisation of [21]. An in depth analysis of the anisotropic stabilisation terms (18) and (20) will be presented in a follow up publication.

3.3. Handling of the non-linearity

To resolve the non-linearity of the full Stokes equations we use a Picard iteration, see Algorithm 1. We chose a Picard iteration over a Newton iteration, since the focus of this paper is not to measure efficiency. Newton iterations are used in ice modelling but requires some extra care due to the viscosity singularity inherent to the full Stokes equations.

In each iteration, the viscosity μ is updated in the viscous term a_h, the ghost penalty and the inf-sup stabilisation term. Note that μ enters in all of the terms of a_h. To our knowledge CutFEM has not been used for a viscosity that varies in space an time. We will show by numerical experiments that simply updating the viscosity in all terms where it appears gives an accurate solution. The resulting linear system is solved using MATLAB's inbuilt backslash operator `mldivide` and the computed velocity is then used in order to update the free surface in the manner described in the next section.

Algorithm 1 General solution procedure. For each time step k and non-linear iteration n a linear system is solved.

1: Set initial condition for velocity $\mathbf{u}_0^0$, pressure p_0^0.
2: **for** $k = 1, \ldots k_{max}$ **do**
3: $n = 1$
4: **while** change $> \epsilon_{tol}$ and $n < 50$ **do**
5: Compute viscosity $\mu_n^k = \mu(\mathbf{u}_n^k)$
6: Assemble linear system from problem (14) using μ_n^k
7: Solve system for velocity $\mathbf{u}_{n+1}^k$ and pressure p_{n+1}^k.
8: calculate change $= \|\mathbf{u}_{n+1}^k - \mathbf{u}_n^k\|_2 / \|\mathbf{u}_{n+1}^k\|_2$
9: $n = n + 1$
10: **end while**
11: Use $\mathbf{u}_n^k$ to update the free surface Γ_s^{k+1}
12: Update the active mesh $\mathcal{T}_h(\Omega)$
13: $k = k + 1$
14: **end for**

4. Time evolution of the ice surface

In order to track the position of the free surface Γ_s we use level set function $\Phi : \Omega_0 \to \mathbb{R}$. It is a signed distance function, so that

$$\begin{cases} \Phi < 0 & \text{if } (x, y) \in \Omega_+, \\ \Phi = 0 & \text{if } (x, y) \in \partial\Omega_+, \\ \Phi > 0 & \text{if } (x, y) \in \Omega_0 \backslash \Omega_+, \end{cases} \tag{21}$$

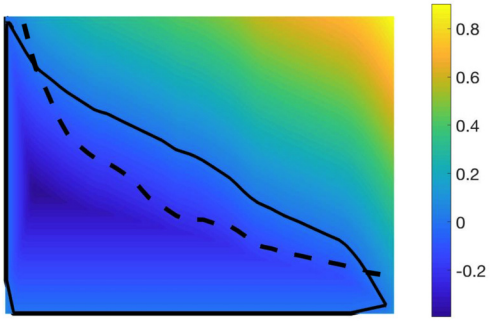

Fig. 4. The level set function Φ (coloured) is zero at the black line, $\partial\Omega_+$. The glacier boundary consists of the parts of this black line and the mountain (dashed line) which lies in between their intersection.

and $|\nabla\Phi| = 1$ at $\partial\Omega_+$. The domain Ω_+ is a domain which is larger than the glacier domain Ω, and whose upper boundary coincides with Γ_s, see the black line in Fig. 4. As the glacier deforms, the level set function is convected by the velocity field according to the free surface equation (4). To account for accumulation/ablation term a_s, we use that $a_s := -a_s^{\perp}\nabla\Phi$ and simply add an extra component $\mathbf{u}_{acc} = [0, a_s^{\perp}]^T$ to the velocity so that (4) can be written as

$$\frac{\partial\Phi}{\partial t} + (\mathbf{u} + \mathbf{u}_{acc}) \cdot \nabla\Phi = 0 \text{ in } \Omega_0. \tag{22}$$

A new glacier boundary $\partial\Omega$ is then defined in the following way. The intersection is found between the line where $\Phi = 0$ (the black line in Fig. 4) and the underlying mountain (the dashed line in Fig. 4). A new Γ_s is then defined as the part of the line $\Phi = 0$ that lies in between the intersection points. In the same way a new Γ_b is defined as the part of the mountain boundary that lies in between the intersection points. In this way the margins (the front and back) of the glacier is free to move. The reason we use a great domain Ω_+ instead of simply having a level set defined by only the extension of Γ_s is purely technical, i.e. it is because the code is written in such a way that the line $\Phi = 0$ is assumed to be a closed polygon. In practice the mountain boundary would be given by data but in this study we find a curve representing the mountain, we extrapolate Γ_b so that it is prolonged to the sides. If the base of the ice would also be moving, e.g. due to subglacial channels, it is possible to represent Γ_b with a level set function. An alternative approach is to define the whole glacier boundary using a level set function, by replacing Ω_+ by Ω in (21), but we found doing so smoothens the sharp edges slightly at the front and back, leading to artificial mass loss.

Note that as the full Stokes equations are only solved in Ω_h, we need to extend the velocity to Ω_0. This is done by solving the Laplace equation in the area outside the glacier with the computed velocity as a Dirichlet condition at $\partial\Omega$ and a homogeneous Neumann condition at $\partial\Omega_0$ (i.e. at the dashed line in Fig. 2). In order to set the boundary conditions, the CutFEM method is again used, with an active domain consisting of the cut elements together with elements completely outside the glacier (the grey coloured elements in Fig. 2). The computational work for solving this problem is small compared to solving the full Stokes equations. The complete velocity field for all of Ω_0 is constructed by combining the two solutions. The extended velocity in nodes within the active glacier mesh $\Omega_h(t)$ (i.e. in the magenta and cyan area of Fig. 2) are given by the full Stokes solution and the solution in the nodes outside the glacier (i.e. belonging only to the grey coloured area in Fig. 2) are given by the solution to the Laplace equation.

In order to retain an accurate representation of the geometry, equation (22) is solved on a mesh twice as fine as the mesh used to solve the full Stokes equations, employing linear interpolation to obtain the velocity $\mathbf{u}_{h/2}$ on the fine mesh. To discretise (22) we use Crank-Nicolson in time and stabilised linear finite elements in space. The discrete problem reads: Find the level-set function $\Phi_{h/2} \in X_{0,h/2}$ such that

$$\left(\frac{\Phi_{h/2}^{n+1} - \Phi_{h/2}^{n}}{\Delta t}, \xi_{h/2}\right) + \frac{1}{2}(\hat{\mathbf{u}}_{h/2}^{n} \cdot \nabla(\Phi_{h/2}^{n+1} + \Phi_{h/2}^{n}), \xi_{h/2}) + \frac{1}{2} s_\Phi(\Phi_{h/2}^{n+1} + \Phi_{h/2}^{n}, \xi_{h/2}) = 0 \quad \forall \xi_{h/2} \in X_{0,h/2}, \tag{23}$$

where $\hat{\mathbf{u}} = \mathbf{u} + \mathbf{u}_{acc}$ and the stabilisation term s_Φ is introduced to control transport instabilities

$$s_\Phi(\Phi_h, \xi_h) = \beta_\Phi \sum_{F \in \mathcal{F}_h(\Omega)} h_n^2 \langle |\hat{\mathbf{u}}_h \cdot \mathbf{n}_F| [\![\mathbf{n}_F \cdot \nabla\Phi_h]\!], [\![\mathbf{n}_F \cdot \nabla\xi_h]\!] \rangle_F, \tag{24}$$

where β_Φ is a user defined parameter. This stabilisation term is the same as in [22], except for that we use the scaling h_n instead of h since this proved more stable in experiments on anisotropic meshes.

In order to identify the new Γ_s, i.e. the line where the level set function Φ is zero and thus changing sign, it is important that $|\nabla\Phi|$ remains close to 1. Therefore the advection of Φ is followed by a reinitialisation step. Available reinitialisation

Table 1
Parameter values used in the numerical experiments.

Description	Notation	Unit square	Arolla glacier
Rate factor ($MPa^{-3}\,year^{-1}$)	A	$2^{\frac{1}{1-p}}$	100
Density ($MPa/(m^2\,year^2)$)	ρ	–	$9.1380 \cdot 10^{-19}$
Gravity ($m/year^2$)	$\mathbf{g}$	–	$[0, -9.7692 \cdot 10^{15}]$
Slip length	ϵ	0	$0, 10^{300}$
Non-linear parameter	$\mathfrak{p}$	4/3	4/3
Critical strain rate	ϵ_{crit}	10^{-7}	10^{-7}
Basal melt rate (m/year)	$a_b^{\perp}$	0	0, 0, 0.01
Surface accumulation (m/year)	$a_s^{\perp}$	0	0, 0.5, 0
Tolerance, non-linear iter.	ϵ_{tol}	10^{-4}	10^{-4}
Mesh resolution	$[h_x, h_y]$	$[2^{-i}, 2^{-i}],\ i = 2, \ldots, 6$	$c\,2^{-4}[\sqrt{8}, \frac{1}{\sqrt{8}}],\ c = 1, 0.75$
Inf-sup stability parameter	α	0.1	10^{-6}
Ghost penalty, velocity	β_u	0.1	1.0
Ghost penalty, pressure	β_p	0.1	0.01
Transport stabilisation par.	β_Φ	-	0.01
Tangential Nitsche penalty	γ_t	0.05	0.005
Normal Nitsche penalty	γ_n	0.05	0.005

techniques tend to smooth very sharp edges, but this is circumvented by introducing Ω_+. To ensure high accuracy we keep the fine mesh $\mathcal{T}_{0,h/2}$ and employ the local projection reinitialisation strategy of [23] at the elements which are cut by the boundary. The local projection reinitialisation is based on finding an exact linear distance function in each element. This procedure gives a globally discontinuous space which is then projected onto a continuous piece wise linear functions. This method works also for unstructured meshes. At elements that are not cut by the boundary the fast sweeping method of [24] is used to extend this distance function iteratively. The final new boundary is $\partial\Omega$ used to define a new active mesh $\mathcal{T}_h(\Omega)$ in the next time step.

5. Numerical experiments

We conduct four numerical experiments, the purpose of which is to show that CutFEM can be used to solve the full Stokes equations and that it is a useful method for simulations of ice dynamics.

Experiment 1a A unit square test in order to verify that the solution converges at the expected rate for the full Stokes equations and is robust with respect to penalty parameters.
Experiment 2a A steady simulation of the Arolla glacier, with no slip conditions at the base.
Experiment 2b A steady simulation of the Arolla glacier with partial slip conditions at the ice bed, representing a subglacial lake found under the glacier.
Experiment 2c A time dependent simulation of Arolla glacier, simulating the free surface evolving between year 1930 and 1932.

The values of all numerical and physical parameters used in these experiments are given in Table 1.

5.1. Experiment 1 - convergence and robustness on a unit square

We follow Example 2 in section 4.8 in [25]. The domain is a unit square $\Omega := (-0.5, 0.5) \times (-0.5, 0.5)$ and the analytical solution is given by

$$u_x = (x^2 + y^2)^{\frac{a-1}{2}} y, \tag{25}$$

$$u_y = -(x^2 + y^2)^{\frac{a-1}{2}} x, \tag{26}$$

$$p = (x^2 + y^2)^{\frac{b}{2}} xy - C. \tag{27}$$

The right hand side of equation (1) is $\mathbf{f} = \nabla \cdot \mathbf{S}(\mathbf{Du}) + \nabla p$ instead of $\rho\mathbf{g}$ and Dirichlet conditions $\mathbf{u}_D = \mathbf{u}|_{\partial\Omega}$ are prescribed on the entire boundary $\partial\Omega$, i.e. $\epsilon = 0$ in (7). To obtain a unique pressure we also enforce the condition $\int_\Omega p\, d\Omega = 0$, implying that $C = \int_\Omega (x^2 + y^2)^{\frac{b}{2}} xy\, d\Omega$ in (25). The rate factor A is set so that $\frac{1}{2}A^{1-p} = 1$ in order to be consistent with [25]. The constants $a, b \in \mathbb{R}$ determine the regularity of the solution. The solution should be regular enough to satisfy $\mathfrak{F}(\mathbf{Du}) := (\epsilon + |\mathbf{Du}|)^{\frac{p-2}{2}} \mathbf{Du} \in W^{1,2}(\Omega)^{2\times 2}$ and $p \in W^{1,p'}$, which corresponds to $a > 1$ and $b > -2/p' - 1$ [16,17,25]. In order to test the method under as difficult conditions as possible we chose $a = 1.01$ and $b = -2/p' - 0.99$, as in [25]. Given these regularity assumptions, optimal convergence estimates

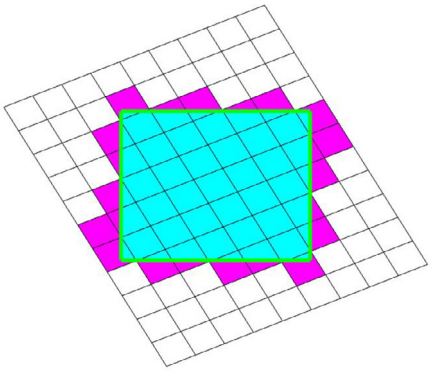

(a) The unit square on the coarsest background mesh

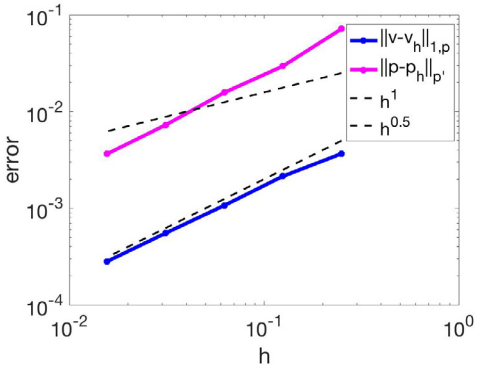

(b) Convergence

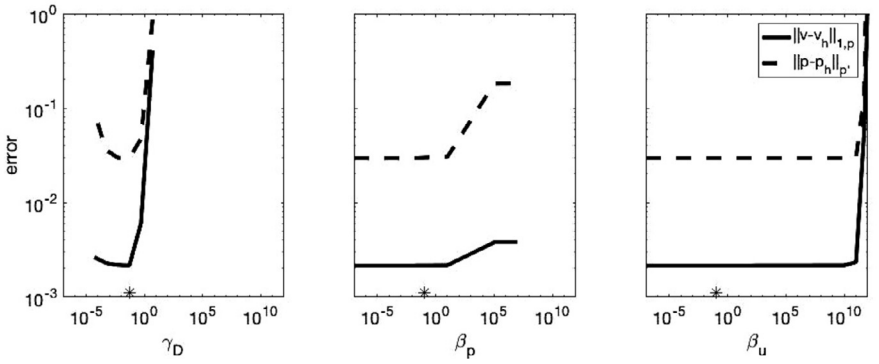

(c) Sensitivity to penalty parameters. The value used for the convergence test is marked by a star.

Fig. 5. Results of Experiment 1 - the unit square test.

$$||\mathbf{u}-\mathbf{u}_h||_{1,\mathfrak{p}} \leq c_u h, \quad ||p-p_h||_{\mathfrak{p}'} \leq c_p h^{2/\mathfrak{p}'}, \tag{28}$$

has been established in the case of $\mathfrak{p} \in (1,2)$ and inf-sup stable elements or first order equal elements stabilised with the local projection stabilisation, for some constants c_u and c_p [16,17,25]. In this experiment we test numerically if the CutFEM solution appear to fulfil similar convergence estimates and how sensitive it is to the choice of the penalty parameters γ_D, β_u, and β_p.

To ensure that cells are cut, the background mesh is rotated with respect to the square with an angle of $\sqrt{2}\pi/4$ radians. For the convergence experiment we then run simulations on a series with meshes with a cellsize $h_x = h_y = 2^{-i}$, $i = 2,3,4,5,6$. The result is shown in Fig. 5b. The velocity converges as expected and the pressure converges faster than the expected rate of $h^{0.5}$.

For the sensitivity study we set $h_x = h_y = 2^{-3}$ and run three sets of experiments. In the first we keep β_u and β_p as in Table 1 and let γ_D take the values $10^{-1}, 1, 10, 10^2, 10^3$, and 10^4. In the second we keep γ_D and β_u as in Table 1 and let β_p take the values $10^{-6}, 10^{-3}, 10^{-1}, 10^2, 10^6$,and 10^8 and in the third we keep γ_D and β_p as in Table 1 and let β_u take the values $10^{-10}, 10^{-6}, 10^{-1}, 10^2, 10^{10}, 10^{11}, 5\cdot 10^{10}$,and 10^{12}. The results are shown in Fig. 5c. The accuracy is not very sensitive to choice of penalty parameters.

5.2. Experiment 2a - the Arolla glacier with no slip conditions

In this experiment we compute the velocity and pressure along a 5 km long central flow line of the Haut Glacier d'Arolla, as it was measured during the Little Ice Age in 1930 (see Fig. 1). The surface and bedrock topography is available on the ISMIP-HOM website [26] with a resolution of 100 m. The physical parameters ρ, $\mathbf{g}$ and A are set according to the ISMIP-HOM benchmark, see Table 1. The background mesh consists of rectangles of width $h_x = 2^{-4}\sqrt{8}$ and height $h_y = 2^{-4}\frac{1}{\sqrt{8}}$, and we scale the problem so that the length unit is km instead of m, in order to ensure that $h_x < 1$.

The computed velocity components and pressure are seen in Fig. 6. The results are in agreement with other full Stokes models in the ISMIP-HOM benchmark, see [15].

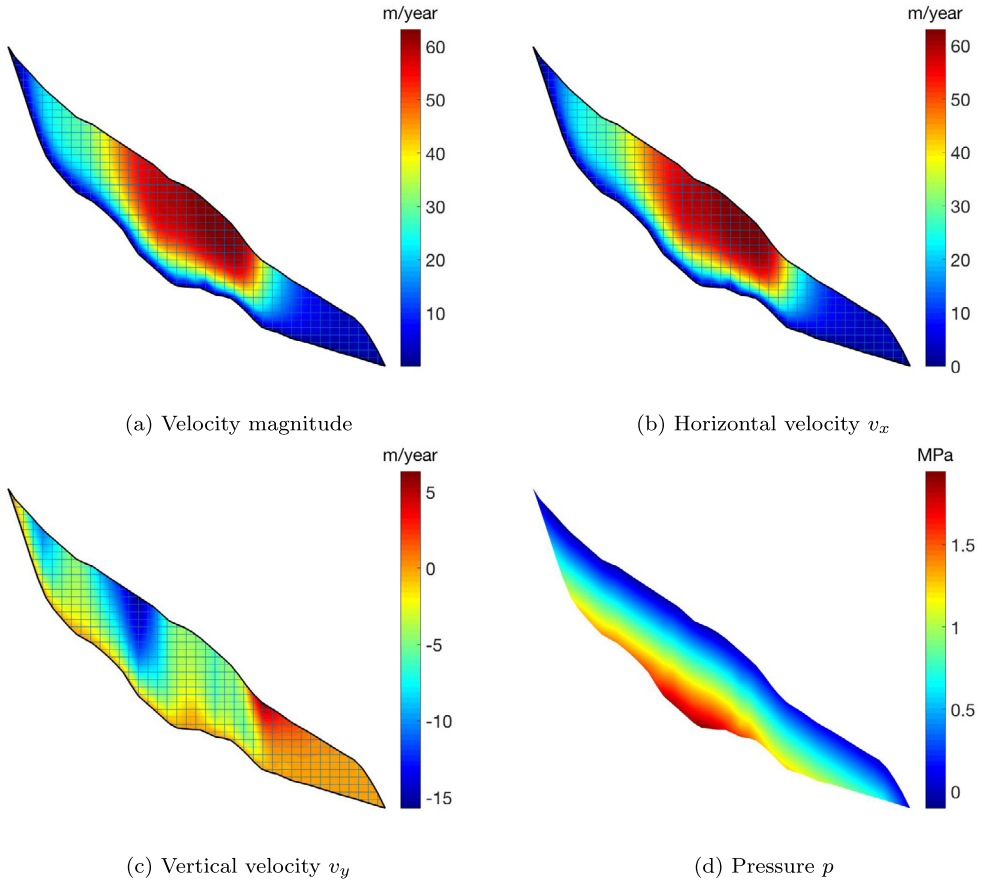

(a) Velocity magnitude

(b) Horizontal velocity v_x

(c) Vertical velocity v_y

(d) Pressure p

Fig. 6. Results of Experiment 2a - Arolla with no slip conditions.

5.3. Experiment 2b - the Arolla glacier with partial slip conditions

In this experiment, we change the basal boundary conditions so that

$$\begin{cases} \epsilon = 10^{300} & \text{if } 2200 \text{ m} \leq x \leq 2500 \text{ m} \\ \epsilon = 0 & \text{elsewhere} \end{cases} \tag{29}$$

These boundary conditions represents subglacial water found under the Arolla glacier as described in the ISMIP-HOM benchmark. The lake is marked blue in Fig. 1. The number 10^{300} is chosen high enough to effectively model $\epsilon \to \infty$, so that there is free slip between the ice and the underlying water. The boundary conditions tests the implementation of the Navier slip conditions and are challenging as they are discontinuous. In order to have more than one mesh node residing in the narrow region of free slip we here refine the mesh slightly in comparison to Experiment 2a, so that $h_x = 0.75 \cdot 2^{-4}\sqrt{8}$ and $h_y = 0.75 \cdot 2^{-4}\frac{1}{\sqrt{8}}$.

The results shown in Fig. 7 are in agreement with other full Stokes models in the ISMIP-HOM benchmark, see [15] and [27], given the relatively coarse resolution here. The coarse resolution used in this paper was chosen to demonstrate the ability to represent geometry without a fine mesh. In practice one can refine the background mesh in selected areas.

5.4. Experiment 2c - time evolution of the Arolla glacier

In the final experiment we let the ice surface evolve from year 1930 to year 1932. This experiment is not part of the ISMIP-HOM benchmark, and we instead compare to the results in [28]. We apply no slip conditions at the base as this is the case in [28]. The time step is 0.2 years. The surface after two years (in 1932) is presented in Fig. 8 together with the initial geometry at 1930. The ice thickness decreases in the upper part of the glacier and the ice accumulates in the lower part, i.e. the glacier is moving down the mountain. The results are in agreement with the results of [28].

In climate related applications, it is important for models to preserve mass. We therefore measure the area changes throughout the simulation, see Fig. 8b. Some area is artificially lost (22.3 m^2), corresponding to about 2 mm artificial surface melt per year, or an relative area change $|A(t=2) - A(t=0)|/A(t=0)$ on the order of 10^{-5}. Given the fairly high

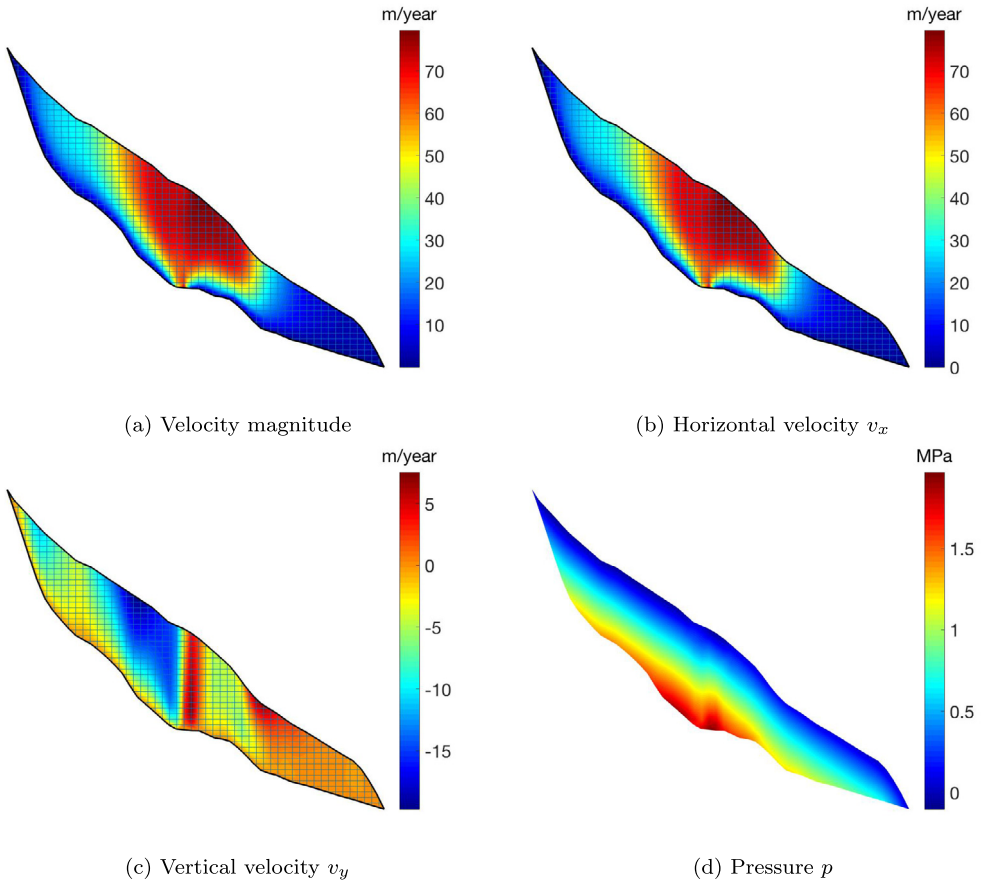

(a) Velocity magnitude

(b) Horizontal velocity v_x

(c) Vertical velocity v_y

(d) Pressure p

Fig. 7. Results of Experiment 2b - the Arolla glacier with partial slip conditions.

non-linear tolerance ϵ_{tol}, coarse mesh and the stabilised equal order linear elements, this is within the expected range. It can be compared to a relative volume change of 10^{-6} for the ice sheet model Elmer/Ice, for an experiment with an ice with constant viscosity is flowing over an artificial sinusoidal bedrock until steady state is reached [29].

Finally, to demonstrate that is possible to model accumulation a_s at the ice surface, as well as basal melt $a_b^\perp$ at the base, we run two more simulations and measure area change. In the first simulation, we model half a meter of accumulation per year over the entire surface by setting $a_s^\perp = 0.5$. Since the length of the glacier changes throughout the simulations slightly (as the front and back moves) it is difficult to calculate exactly how large the area change should be. On average the glacier length is however about 4890.1 m long, meaning that the glacier should in two years gain 4890.1 m ·0.5 m/year ·2 years $= 4890.1$ m^2. This agrees with the measured area gain of 4877.6 m^2, considering that the numerical error is about 20 m^2 (see Fig. 8b). It should be noted that in reality the accumulation on the Arolla glacier is about -2 m [30]. In the second simulation, we set a basal melt $a_b^\perp = 0.01$ m/year, i.e. we set $\mathbf{g}_d = (0, -0.01)$. This should result in a area *loss* of 4890.1 m ·0.01 m/year ·2 years $=$ 97.8 m^2, which also agrees well with the measured area loss of 120.2 m^2, again considering the numerical error.

6. Summary and conclusion

The unfitted sharp interface finite element method CutFEM has been applied to simulate glaciers in two dimensions. A strategy for handling non-linear viscosities, thin domains, variable slip conditions and an evolving domain with sharp edges has been developed. The order of convergence is at least as high as expected from finite element theory for non-Newtonian fluids. The method produces accurate velocity and pressure profiles for the Swiss glacier Haut Glacier d'Arolla, for fully frozen basal conditions as well as for an underlying subglacial lake. The deformation of the glacier from year 1930 to 1932 has been simulated with and without basal melt and surface accumulation, showing that the movement of the glacier surface is well modelled despite not being represented by mesh nodes.

The CutFEM method appears to be a viable option for ice dynamics simulations which avoids issues with meshing and remeshing. The CutFEM method has been implemented in three dimensions in mature softwares such as deal.II and FEniCS [31,32] so that en extension to large scale three dimensional ice sheet simulations is possible by following the same

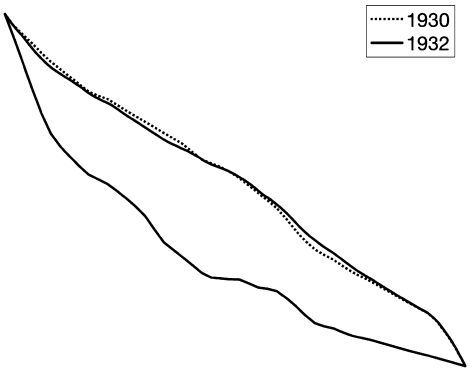

(a) The outline of the Arolla glacier in year 1930 and 1932, with $a_s^\perp = a_b^\perp = 0$.

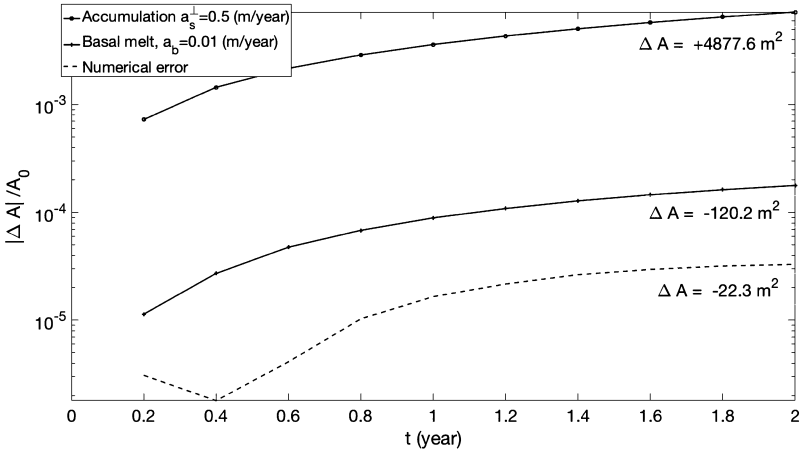

(b) Area change over time for three different simulations: one with no external mass contribution ($a_s^\perp = a_b^\perp = 0$), one with surface accumulation ($a_s^\perp = 0.5$ m/year), and one with basal melt ($a_b^\perp = 0.01$ m/year).

Fig. 8. Results of Experiment 2c - transient simulations of the Arolla glacier.

procedure as in this paper. Other interesting extensions of this study are marine terminating glaciers, configurations with topological changes, as well as performance comparisons to classical fitted FEM on large scale problems.

CRediT authorship contribution statement

Josefin Ahlkrona: Conceptualization, Formal analysis, Investigation, Methodology, Software, Visualization, Writing – original draft. **Daniel Elfverson:** Conceptualization, Formal analysis, Investigation, Methodology, Software, Writing – review & editing.

Declaration of competing interest

The authors declare that they have no known competing financial interests or personal relationships that could have appeared to influence the work reported in this paper.

Acknowledgements

The authors acknowledge the funding provided by the Swedish e-Science Research Centre (SeRC). Part of the research was conducted during a research visit at Kiel University, funded by the Cluster of Excellence 80 “The Future Ocean”. The “Future Ocean” is funded within the framework of the Excellence Initiative by the Deutsche Forschungsgemeinschaft (DFG) on behalf of the German federal and state governments. We are grateful for fruitful discussions with Christian Helanow and to the anonymous reviewer who thoroughly read the manuscript and whose suggestions of additional numerical experiments improved the study significantly.

References

[1] J. Church, P. Clark, A. Cazenave, J. Gregory, S. Jevrejeva, A. Levermann, M. Merrifield, G. Milne, R. Nerem, P. Nunn, A. Payne, W. Pfeffer, D. Stammer, A. Unnikrishnan, Climate Change 2013: The Physical Science Basis. Contribution of Working Group I to the Fifth Assessment Report of the Intergovernmental Panel on Climate Change, Cambridge University Press, Cambridge, United Kingdom and New York, NY, USA, 2013, pp. 1137–1216.

[2] H.-O. Pörtner, D. Roberts, V. Masson-Delmotte, P. Zhai, M. Tignor, E. Poloczanska, K. Mintenbeck, A. Alegría, M. Nicolai, A. Okem, J. Petzold, B. Rama, N.e. Weyer, IPCC Special Report on the Ocean and Cryosphere in a Changing Climate, 2019, in press, https://www.ipcc.ch/srocc/.

[3] E. Larour, H. Seroussi, M. Morlighem, E. Rignot, Continental scale, high order, high spatial resolution, ice sheet modeling using the Ice Sheet System Model (ISSM), J. Geophys. Res., Earth Surf. 117 (2012), https://doi.org/10.1029/2011JF002140.

[4] N. Petra, H. Zhu, G. Stadler, T.J.R. Hughes, O. Ghattas, An inexact Gauss-Newton method for inversion of basal sliding and rheology parameters in a nonlinear Stokes ice sheet model, J. Glaciol. 58 (2012) 889–903, https://doi.org/10.3189/2012JoG11J182.

[5] D.J. Brinkerhoff, J.V. Johnson, Data assimilation and prognostic whole ice sheet modelling with the variationally derived, higher order, open source, and fully parallel ice sheet model VarGlaS, Cryosphere 7 (2013) 1161–1184, https://doi.org/10.5194/tc-7-1161-2013.

[6] O. Gagliardini, T. Zwinger, et al., Capabilities and performance of Elmer/Ice, a new generation ice-sheet model, Geosci. Model Dev. 6 (2013) 1299–1318, https://doi.org/10.5194/gmd-6-1299-2013.

[7] E. Burman, S. Claus, P. Hansbo, M.G. Larson, A. Massing, Cutfem: discretizing geometry and partial differential equations, Int. J. Numer. Methods Eng. 104 (2015) 472–501, https://doi.org/10.1002/nme.4823.

[8] T.-P. Fries, T. Belytschko, The extended/generalized finite element method: an overview of the method and its applications, Int. J. Numer. Methods Eng. 84 (2010) 253–304, https://doi.org/10.1002/nme.2914.

[9] J. Nitsche, Über ein Variationsprinzip zur Lösung von Dirichlet-Problemen bei Verwendung von Teilräumen, die keinen Randbedingungen unterworfen sind, Abh. Math. Semin. Univ. Hamb. 36 (1971) 9–15, https://doi.org/10.1007/bf02995904.

[10] A. Hansbo, P. Hansbo, An unfitted finite element method, based on Nitsche's method, for elliptic interface problems, Comput. Methods Appl. Mech. Eng. 191 (2002) 5537–5552, https://doi.org/10.1016/S0045-7825(02)00524-8.

[11] A. Massing, M.G. Larson, A. Logg, M.E. Rognes, A stabilized Nitsche fictitious domain method for the Stokes problem, J. Sci. Comput. 61 (2014) 604–628, https://doi.org/10.1007/s10915-014-9838-9.

[12] T. Frachon, S. Zahedi, A cut finite element method for incompressible two-phase Navier–Stokes flows, J. Comput. Phys. 384 (2019) 77–98, https://doi.org/10.1016/j.jcp.2019.01.028.

[13] G. Cheng, P. Lötstedt, L. von Sydow, A full Stokes subgrid scheme in two dimensions for simulation of grounding line migration in ice sheets using Elmer/ICE (v8.3), Geosci. Model Dev. 13 (2020) 2245–2258, https://doi.org/10.5194/gmd-13-2245-2020.

[14] J.H. Bondzio, H. Seroussi, M. Morlighem, T. Kleiner, M. Rückamp, A. Humbert, E.Y. Larour, Modelling calving front dynamics using a level-set method: application to Jakobshavn Isbræ, West Greenland, Cryosphere 10 (2016) 497–510, https://doi.org/10.5194/tc-10-497-2016.

[15] F. Pattyn, L. Perichon, A. Aschwanden, B. Breuer, B. de Smedt, O. Gagliardini, G.H. Gudmundsson, R. Hindmarsh, A. Hubbard, J.V. Johnson, T. Kleiner, Y. Konovalov, C. Martin, A.J. Payne, D. Pollard, S. Price, M. Rückamp, F. Saito, O. Souček, S. Sugiyama, T. Zwinger, Benchmark experiments for higher-order and full-Stokes ice sheet models (ISMIP-HOM), Cryosphere 2 (2008) 95–108, https://doi.org/10.5194/tc-2-95-2008.

[16] L. Belenki, L.C. Berselli, L. Diening, M. Růžička, On the finite element approximation of p-Stokes systems, SIAM J. Numer. Anal. 50 (2012) 373–397, https://doi.org/10.2307/41582741.

[17] A. Hirn, Approximation of the p-Stokes equations with equal-order finite elements, J. Math. Fluid Mech. 15 (2012) 65–88, https://doi.org/10.1007/s00021-012-0095-0.

[18] M. Winter, B. Schott, A. Massing, W. Wall, A Nitsche cut finite element method for the Oseen problem with general Navier boundary conditions, Comput. Methods Appl. Mech. Eng. 330 (2018) 220–252, https://doi.org/10.1016/j.cma.2017.10.023.

[19] E. Burman, A. Ern, Continuous interior penalty hp-finite element methods for advection and advection-diffusion equations, Math. Comput. 76 (2007) 1119–1140, https://doi.org/10.1090/S0025-5718-07-01951-5.

[20] D. Boffi, M. Fortin, F. Brezzi, Mixed Finite Element Methods and Applications, Springer Series in Computational Mathematics, Springer, Berlin, Heidelberg, 2013.

[21] S. Frei, An edge-based pressure stabilization technique for finite elements on arbitrarily anisotropic meshes, Int. J. Numer. Methods Fluids 89 (2019) 407–429, https://doi.org/10.1002/fld.4701.

[22] E. Burman, M.A. Fernández, Continuous interior penalty finite element method for the transient convection-diffusion-reaction equation, Research Report RR-6543, Inria, French Institute for Research in Computer Science and Automation, 2008.

[23] N. Parolini, E. Burman, A local projection reinitialization procedure for the level set equation on unstructured grids, Technical Report CMCS-REPORT-2007-004, École Polytechnique Fédérale de Lausanne, 2007.

[24] Y.-H.R. Tsai, L.-T. Cheng, S. Osher, H.-K. Zhao, Fast sweeping algorithms for a class of Hamilton—Jacobi equations, SIAM J. Numer. Anal. 42 (2003) 673–694, https://doi.org/10.1137/S0036142901396533.

[25] A. Hirn, Finite element approximation of problems in non-Newtonian fluid mechanics, Ph.D. thesis, Naturwissenschaftlich-Mathematischen Gesamtfakultät der Ruprecht-Karls-Universität Heidelberg und der Mathematisch-Physikalischen Fakultät der Karls-Universität Prag, 2011.

[26] F. Pattyn, ISMIP-HOM benchmark website, http://homepages.ulb.ac.be/~fpattyn/ismip/. (Accessed 30 June 2019).

[27] C. Helanow, Effects of numerical implementations of the impenetrability condition on non-linear Stokes flow: applications to ice dynamics, e-prints, arXiv:1907.12315, 2019.

[28] J. Ahlkrona, V. Shcherbakov, A meshfree approach to non-Newtonian free surface ice flow: application to the Haut Glacier d'Arolla, J. Comput. Phys. 330 (2017) 633–649, https://doi.org/10.1016/j.jcp.2016.10.045.

[29] O. Gagliardini, T. Zwinger, The ISMIP-HOM benchmark experiments performed using the finite-element code Elmer, Cryosphere 2 (2008) 67–76, https://doi.org/10.5194/tc-2-67-2008.

[30] R. Dadic, J.G. Corripio, P. Burlando, Mass-balance estimates for Haut Glacier d'Arolla, Switzerland, from 2000 to 2006 using dems and distributed mass-balance modeling, Ann. Glaciol. 49 (2008) 22–26, https://doi.org/10.3189/172756408787814816.

[31] C. Gürkan, S. Sticko, A. Massing, Stabilized cut discontinuous Galerkin methods for advection-reaction problems, SIAM J. Sci. Comput. 42 (2020) A2620–A2654, https://doi.org/10.1137/18M1206461.

[32] A. Massing, B. Schott, W. Wall, A stabilized Nitsche cut finite element method for the Oseen problem, Comput. Methods Appl. Mech. Eng. 328 (2018) 262–300, https://doi.org/10.1016/j.cma.2017.09.003.